

# Dependence model assessment and selection with DecoupleNets

Marius Hofert<sup>1</sup>, Avinash Prasad<sup>2</sup>, Mu Zhu<sup>3</sup>

2022-10-06

Neural networks are suggested for learning a map from  $d$ -dimensional samples with any underlying dependence structure to multivariate uniformity in  $d'$  dimensions. This map, termed DecoupleNet, is used for dependence model assessment and selection. If the data-generating dependence model was known, and if it was among the few analytically tractable ones, one such transformation for  $d' = d$  is Rosenblatt's transform. DecoupleNets have multiple advantages. For example, they only require an available sample and are applicable to  $d' < d$ , in particular  $d' = 2$ . This allows for simpler model assessment and selection, both numerically and, because  $d' = 2$ , especially graphically. A graphical assessment method has the advantage of being able to identify why, or in which region of the domain, a candidate model does not provide an adequate fit, thus leading to model selection in particular regions of interest or improved model building strategies in such regions. Through simulation studies with data from various copulas, the feasibility and validity of this novel DecoupleNet approach is demonstrated. Applications to real world data illustrate its usefulness for model assessment and selection.

## Keywords

Neural networks, copulas, Rosenblatt transformation, model assessment, model selection, graphical approach.

## MSC2010

62H99, 65C60, 60E05, 62M45, 00A72, 65C10, 62M10.

## 1 Introduction

Copula modeling is well established by now, be it for parameter estimation in statistical applications to engineering or hydrology, or for model building in applications to finance, insurance or risk management, to name a few. The quest to find an adequate copula for the modeling task at hand is omnipresent, especially in higher-dimensional applications, where the application of interest defines what constitutes “higher-dimensional”; see, for example, Hofert and Oldford (2018) where even the most commonly applied copula models fail to adequately capture the dependence found in basic log-return data. In this paper, we present an approach to help the dependence modeler in that quest. Moreover, and in contrast to other assessment methods – for example, purely numerically in terms of single numbers based on test statistics (for example, Genest et al. 2009) or graphically

---

<sup>1</sup>Department of Statistics and Actuarial Science, University of Waterloo, 200 University Avenue West, Waterloo, ON, N2L 3G1, [marius.hofert@uwaterloo.ca](mailto:marius.hofert@uwaterloo.ca). The author acknowledges support from NSERC (Grant RGPIN-2020-04897).

<sup>2</sup>Department of Statistics and Actuarial Science, University of Waterloo, 200 University Avenue West, Waterloo, ON, N2L 3G1, [a2prasad@uwaterloo.ca](mailto:a2prasad@uwaterloo.ca).

<sup>3</sup>Department of Statistics and Actuarial Science, University of Waterloo, 200 University Avenue West, Waterloo, ON, N2L 3G1, [mu.zhu@uwaterloo.ca](mailto:mu.zhu@uwaterloo.ca). The author acknowledges support from NSERC (RGPIN-2016-03876).

through pairs only (for example, Hofert and Mächler 2014; Hofert and Oldford 2018), if a copula model is not deemed adequate, our approach can give guidance why, for example in which tail region, the model fails to capture dependence properly.

If  $\mathbf{U} \sim C$  for a  $d$ -dimensional copula  $C$ , the central idea of our paper is to introduce a *DecoupleNet*, a neural network to be specified later, which maps  $\mathbf{U}$  to  $\mathbf{U}' \sim U(0, 1)^{d'}$  for  $d' \leq d$ . The flexibility of DecoupleNets allows us to learn transformations not only from any (non-tractable) parametric copula  $C$ , but also from any underlying empirical copula of a given dataset. A DecoupleNet is thus a natural tool for answering the question

“How can we assess and select copulas that best fit given data?”

In Section 2 we introduce DecoupleNets and our approach for dependence model assessment and selection. As a high-level and easy to grasp graphical example for  $d = d' = 2$  in this introduction, we trained a DecoupleNet, denoted by  $D_{2,2}^{C_{4,0.4}^t}$ , on a sample of size 50 000 from a bivariate  $t$  copula with  $\nu = 4$  degrees of freedom and Kendall’s tau being  $\tau = 0.4$ ; in short,  $C = C_{\nu,\tau}^t = C_{4,0.4}^t$  (for notational ease, we omit incorporating the dimension in the notation of copulas in this work, as it should be clear from the context). The top left plot of Figure 1 shows a (new) sample of size  $n_{\text{gen}} = 5000$  from this copula. Passing this sample through  $D_{2,2}^{C_{4,0.4}^t}$  leads to the bottom left plot whose uniformity confirms training quality. In the top right plot, we see a sample of size 5000 from some candidate model – here, a Clayton copula with the same Kendall’s tau  $\tau = 0.4$  – whose adequacy for the training data we want to assess. Applying  $D_{2,2}^{C_{4,0.4}^t}$  to this sample leads to the plot on the bottom right. We clearly see departure from uniformity suggesting that this Clayton copula is not an adequate model for our data; we will later also color points belonging to specific regions of interest so that model assessment and selection can also be focused on specific regions. Repeating this procedure for several candidate models allows us to assess them and select the most suitable one. As we will see later, the same holds true if  $d > d' = 2$ , which makes this graphical assessment and selection approach feasible in higher dimensions. To complement the graphical assessment, the quality of overall (non-)uniformity can also be summarized numerically. Section 3 investigates the details of the graphical approach and the numerical summary in terms of simulated data. Another advantage of DecoupleNets is that they can capture the dependence of any real world data; see Section 4. Moreover, the perceived computational burden of having to train a neural network can become negligible in comparison to having to find parametric candidate models, estimate their parameters and compute quantities such as the Rosenblatt transform for model assessment and selection (if available at all). Section 5 concludes with a summary and outlook.

## 2 DecoupleNets for model assessment and selection

### 2.1 Transformation

Let  $C$  be any  $d$ -dimensional copula. A *DecoupleNet*  $D_{d,d'}^C$  is a neural network that maps  $\mathbf{U} \sim C$  to  $\mathbf{U}' \sim U(0, 1)^{d'}$ , so  $D_{d,d'}^C(\mathbf{U}) = \mathbf{U}'$  with the goal of model assessment and selection. We specify this map to be  $D_{d,d'}^C = T^C \circ \Phi^{-1}$ , where  $\Phi^{-1}(\mathbf{u}) = (\Phi^{-1}(u_1), \dots, \Phi^{-1}(u_d))$  is a componentwise transformation with the standard normal quantile function  $\Phi^{-1}$  and  $T^C$  is a trained neural network. The initial map  $\Phi^{-1}$  to standard normal margins acts as a pre-processing step that helps facilitate the training of the neural network  $T^C$ .

**Remark 2.1 (Rosenblatt’s transformation)**

Another transformation from  $\mathbf{U} \sim C$  to  $\mathbf{U}' \sim U(0, 1)^{d'}$ , but limited to  $d' = d$ , is the transformation

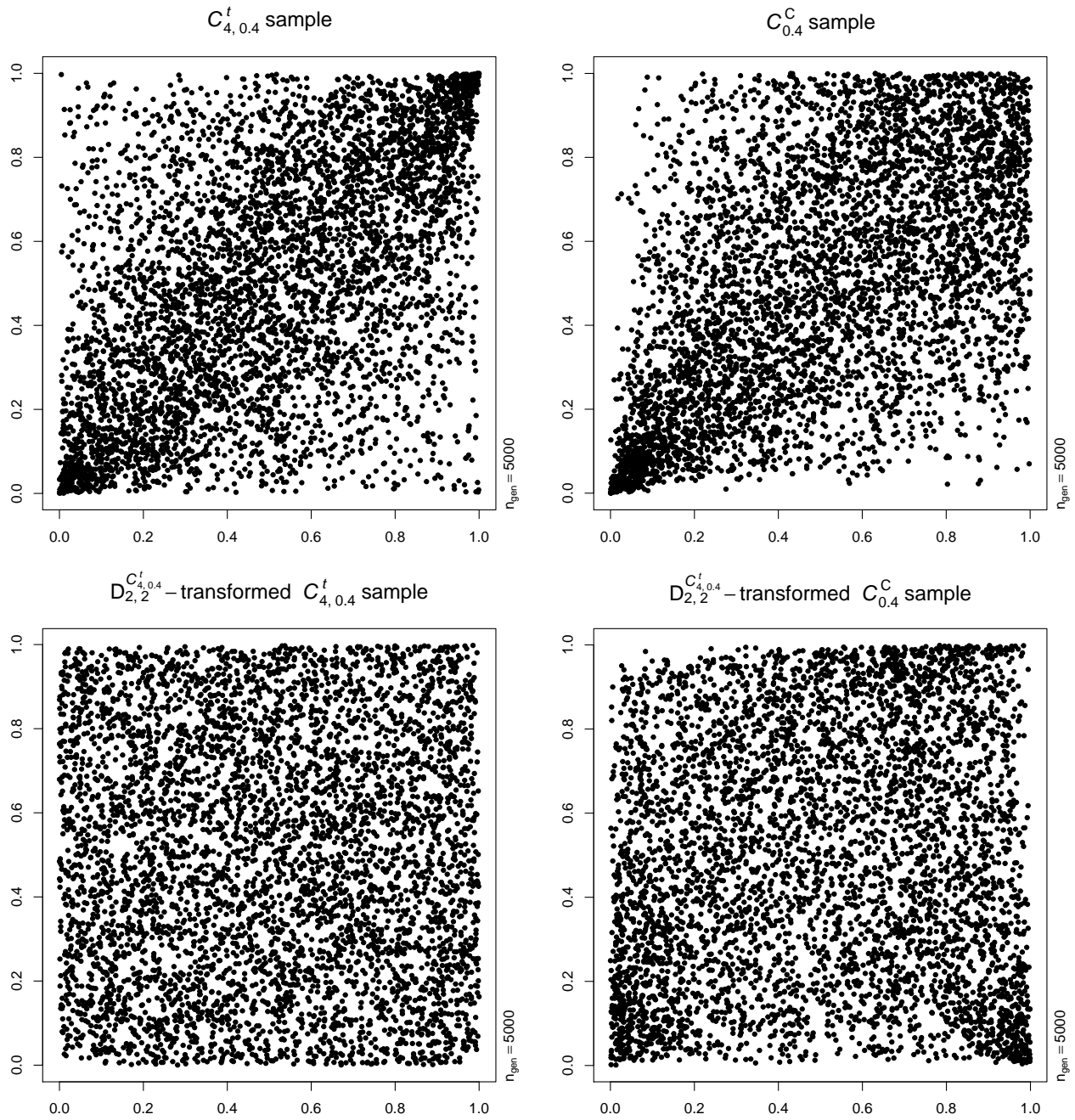


**Figure 1** Samples of size  $n_{\text{gen}} = 5000$  from a bivariate  $C_{4,0.4}^t$  copula (top left) and a bivariate  $C_{0.4}^C$  copula (top right), with corresponding  $D_{2,2}^{C_{4,0.4}^t}$ -transformed samples (bottom row).

of Rosenblatt (1952). It is the (only known) general such transformation from  $\mathbf{U} \sim C$  (the “general” referring to the fact that it applies to any  $d$ -dimensional copula  $C$ ) to  $\mathbf{U}' \sim \text{U}(0, 1)^d$ ; for specific  $C$ , there may be other transformations, for example the one of Wu et al. (2007) for Archimedean copulas. Having to rely on such transformations has several main drawbacks in comparison to DecoupleNets. First, for any  $d$ -dimensional copula  $C$ , Rosenblatt’s transformation is given by  $\mathbf{U}' = R_d^C(\mathbf{U})$  with first component  $R_d^C(\mathbf{U})_1 = U_1$  and  $j$ th component

$$R_d^C(\mathbf{U})_j = C_{j|1,\dots,j-1}(U_j | U_1, \dots, U_{j-1}), \quad j = 2, \dots, d;$$

here  $C_{j|1,\dots,j-1}(u_j | u_1, \dots, u_{j-1}) = \mathbb{P}(U_j \leq u_j | U_1 = u_1, \dots, U_{j-1} = u_{j-1})$ . Under differentiability assumptions on  $C$ , these conditional distributions can be expressed as

$$C_{j|1,\dots,j-1}(u_j | u_1, \dots, u_{j-1}) = \frac{\frac{\partial^{j-1}}{\partial x_{j-1} \dots \partial x_1} C^{(1,\dots,j)}(x_1, \dots, x_j) \Big|_{(x_1, \dots, x_j) = (u_1, \dots, u_j)}}{\frac{\partial^{j-1}}{\partial x_{j-1} \dots \partial x_1} C^{(1,\dots,j-1)}(x_1, \dots, x_{j-1}) \Big|_{(x_1, \dots, x_{j-1}) = (u_1, \dots, u_{j-1})}} \quad (1)$$

For most copulas, (1) is not available analytically, nor tractable numerically. Notable exceptions where (1) is available are normal,  $t$  and Clayton copulas. However, these copulas are typically not flexible enough to fit real world data well, the second drawback. This especially applies to higher dimensions where, additionally, the fact that  $d' = d$  makes computing (1) numerically and computationally intractable, the third drawback. Despite these drawbacks, Rosenblatt’s transformation is applied in copula modeling; see, for example, Genest et al. (2009).

As we will see, DecoupleNets have none of these drawbacks. Moreover, although run time is not a focus here, note that the perceived computational burden of having to train a neural network is well compensated by considering the only available (but largely limited) alternative, such as the Rosenblatt transform (for  $d' = d$ ). In virtually all applications, we do *not* know the true underlying copula, so we would first need to estimate various candidate models and then compute their (implied) Rosenblatt transforms, etc. In this light, having to train just one neural network is actually orders of magnitudes faster. Furthermore, the training of the rather simple neural networks we use is by no means very time-consuming (especially also with the rather small sample sizes one often faces in practice).

Furthermore, the copula  $C$  underlying  $D_{d,d'}^C$  is typically not known analytically and only specified through a given sample.

## 2.2 Optimization

To train a DecoupleNet, we make use of a generative neural network modeling technique introduced by Li et al. (2015) and Dziugaite et al. (2015). We work with a family  $\mathcal{T}$  of feedforward neural networks with a pre-specified architecture, where a network  $T^C \in \mathcal{T}$  is characterized by weights  $\mathbf{W}$ . Given a sample  $\{\mathbf{U}_i\}_{i=1}^{n_{\text{trn}}}$  from  $C$  and a sample  $\{\mathbf{U}'_i\}_{i=1}^{n_{\text{trn}}}$  from  $\text{U}(0, 1)^d$ , we minimize

$$\begin{aligned} & \mathcal{L}\left(\{T^C(\Phi^{-1}(\mathbf{U}_i))\}_{i=1}^{n_{\text{trn}}}, \{\mathbf{U}'_i\}_{i=1}^{n_{\text{trn}}}\right) \\ &= \frac{1}{n_{\text{trn}}^2} \sum_{i=1}^{n_{\text{trn}}} \sum_{i'=1}^{n_{\text{trn}}} \left( K(T^C(\Phi^{-1}(\mathbf{U}_i)), T^C(\Phi^{-1}(\mathbf{U}_{i'}))) - 2K(T^C(\Phi^{-1}(\mathbf{U}_{i'})), \mathbf{U}'_i) + K(\mathbf{U}'_i, \mathbf{U}'_{i'}) \right) \end{aligned} \quad (2)$$

over all  $T^C \in \mathcal{T}$  by a version of stochastic gradient descent, where  $K(\cdot, \cdot)$  is a kernel function. Minimizing (2) ensures that the distribution of the DecoupleNet output  $\{D_{d,d'}^C(\mathbf{U}_i)\}_{i=1}^{n_{\text{trn}}}$  is as close as possible to  $\text{U}(0, 1)^d$ . This is due to the fact that the loss function  $\mathcal{L}$  being minimized is equal to

$$\left\| \frac{1}{n_{\text{trn}}} \sum_{i'=1}^{n_{\text{trn}}} \varphi(T^C(\Phi^{-1}(\mathbf{U}_{i'}))) - \frac{1}{n_{\text{trn}}} \sum_{i=1}^{n_{\text{trn}}} \varphi(\mathbf{U}'_i) \right\|^2, \quad (3)$$

where  $\varphi$  is the implied feature map of  $K$ , such that  $K(\mathbf{u}, \mathbf{v}) = \varphi(\mathbf{u})^\top \varphi(\mathbf{v})$ . By selecting  $K$  to be a Gaussian kernel  $K(\mathbf{u}, \mathbf{v}) = \exp(-\|\mathbf{u} - \mathbf{v}\|^2/\sigma)$ , where  $\sigma > 0$  denotes the bandwidth parameter, the two terms in (3) will contain all empirical moments of  $\{D_{d,d'}^C(\mathbf{U}_\ell)\}_{\ell=1}^{n_{\text{trn}}}$  and  $\{\mathbf{U}'_i\}_{i=1}^{n_{\text{trn}}}$ , respectively, thus ensuring that the DecoupleNet output matches the  $U(0, 1)^{d'}$  distribution. For more details about the types of generative neural networks we use (that is,  $T^C$  in (2)) and their capabilities for learning maps between uniformity and (possibly empirically) specified dependencies, see Hofert, Prasad, et al. (2021b). As in this reference, we follow the suggestion of Li et al. (2015) and work with a mixture of Gaussian kernels with different bandwidth parameters in order to avoid selecting a single optimal bandwidth parameter.

### 2.3 Training

Directly performing the optimization in (2), also known as *batch optimization*, would involve all  $\binom{n_{\text{trn}}}{2}$  pairs of observations which is memory-prohibitive even for moderately large  $n_{\text{trn}}$ . Instead, we adopt a *mini-batch optimization* procedure, where the training dataset is partitioned into *batches* of size  $n_{\text{bat}}$  and the batches are used sequentially to update the weights  $\mathbf{W}$  with the Adam optimizer of Kingma and Ba (2014) (a “memory-sticking gradient” procedure, that is a weighted combination of the current gradient and past gradients from earlier iterations). After a pass through the entire training data, that is, after roughly  $(n_{\text{trn}}/n_{\text{bat}})$ -many gradient steps, one *epoch* of the neural network training is completed. The trade-off in utilizing mini-batches, particularly with a smaller batch size  $n_{\text{bat}}$ , is that the objective function is computed only with partial information for each gradient step in the optimization. For relatively small datasets however batch optimization can still be used, and conceptually we can view it as a special case of the mini-batch procedure (for  $n_{\text{bat}} = n_{\text{trn}}$ ).

### 2.4 Understanding DecoupleNets and how to use them for dependence model assessment and selection

We now briefly revisit the example of Section 1 to illustrate the nature of a trained DecoupleNet transform and why it is useful for model assessment and selection.

By construction, given an input sample  $\{\mathbf{U}_i\}_{i=1}^{n_{\text{gen}}}$  from a known copula (or pseudo-observations of an unknown copula)  $C$ , the trained DecoupleNet  $D_{d,d'}^C$  generates an output sample  $\{D_{d,d'}^C(\mathbf{U}_i)\}_{i=1}^{n_{\text{gen}}}$  that is approximately  $U(0, 1)^{d'}$ . On the other hand, for an input sample  $\{\tilde{\mathbf{U}}_i\}_{i=1}^{n_{\text{gen}}}$  from some candidate copula  $\tilde{C}$  with  $\tilde{C} \neq C$ , the DecoupleNet output  $\{D_{d,d'}^C(\tilde{\mathbf{U}}_i)\}_{i=1}^{n_{\text{gen}}}$  should exhibit departures from  $U(0, 1)^{d'}$ .

To demonstrate this idea, Figure 2 shows the same data as Figure 1 but we now colored different regions of the input samples  $\{\mathbf{U}_i\}_{i=1}^{n_{\text{gen}}}$  and, correspondingly, the output samples  $\{D_{2,2}^{C_{4,0.4}^t}(\mathbf{U}_i)\}_{i=1}^{n_{\text{gen}}}$ . Comparing the plot on the bottom left with the one on the top left, we see from the colored regions that samples  $\{\mathbf{U}_i\}_{i=1}^{n_{\text{gen}}}$  in the joint right tail of  $C_{4,0.4}^t$  are (here) mapped to samples  $\{D_{2,2}^{C_{4,0.4}^t}(\mathbf{U}_i)\}_{i=1}^{n_{\text{gen}}}$  that concentrate near the bottom (small second component), and similarly for the joint left tail. Comparing the plot on the bottom right with the one on the bottom left, we see that the region at the bottom (with samples from the joint right tail) is underrepresented, so there must have been too few input samples in the upper right region – indeed what we see in the plot at the top right in comparison to the one on the top left; one can also verify this numerically, the probability to fall in  $[6/7, 1]^2$  is about 0.0673 under  $C_{4,0.4}^t$  and about 0.0400 under  $C_{0.4}^C$ . Similarly, the region at the top with samples from the joint left tail is overrepresented, so there must have been too many input samples in the lower left region – indeed what we see in the plot at the top right in comparison to the one on the top left; and again one can verify this numerically, the probability to fall in  $[0, 1/7]^2$

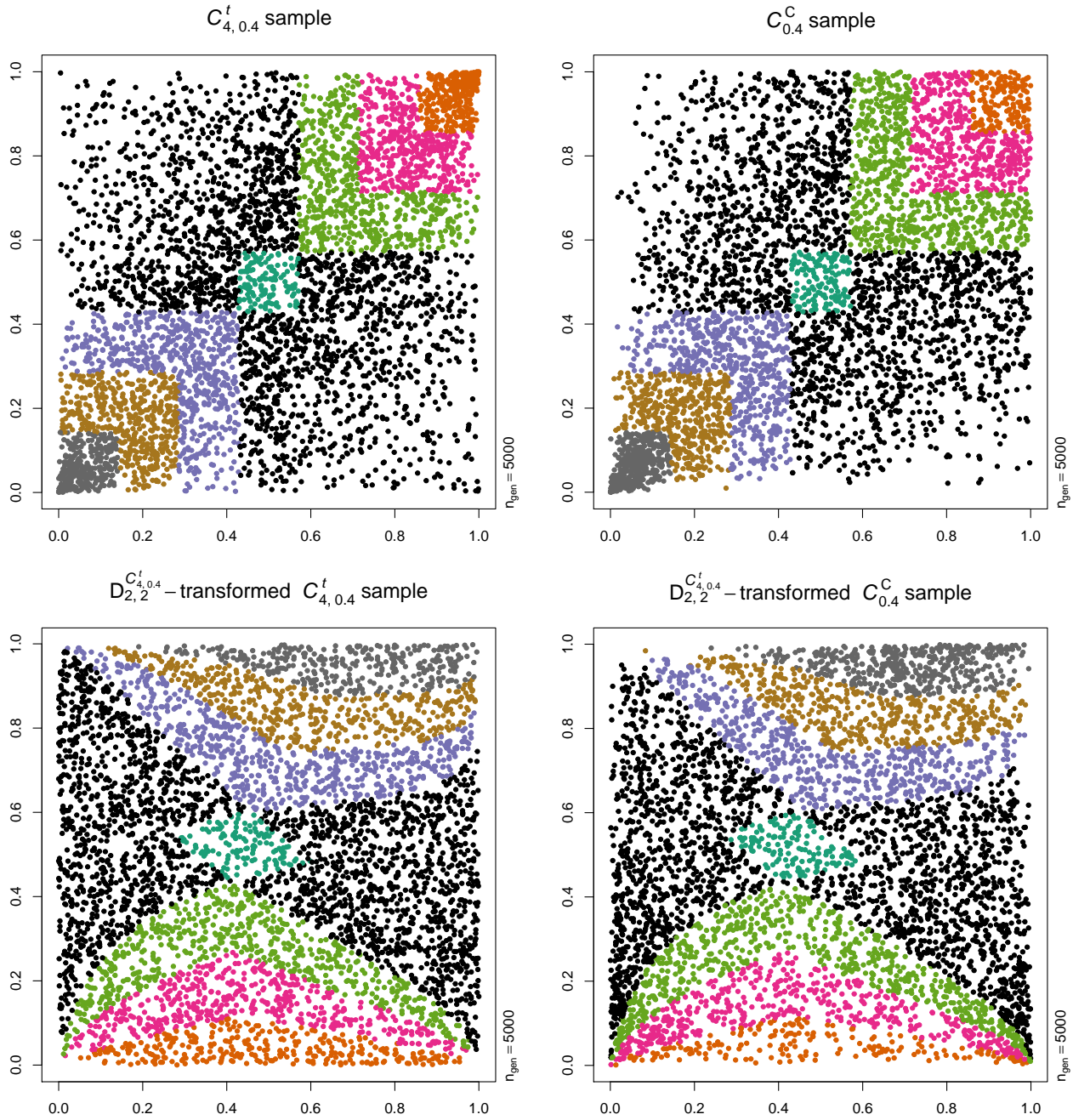


**Figure 2** Colored samples of size  $n_{\text{gen}} = 5000$  from a bivariate  $C_{4,0.4}^t$  copula (top left) and a bivariate  $C_{0.4}^C$  copula (top right), with corresponding  $D_{2,2}^{C_{4,0.4}^t}$ -transformed samples (bottom row).

is about 0.0673 under  $C_{4,0.4}^t$  and about 0.0874 under  $C_{0.4}^C$ . In short, the colors indicate to which regions input samples are transformed and thus allow us to assess and select copulas that well capture specific regions of interest.

Figure 3 shows  $D_{3,2}^{C_{4,0.4}^t}$ -transformed colored samples from a  $C_{4,0.4}^t$  and a  $C_{0.4}^C$  copula. This is an

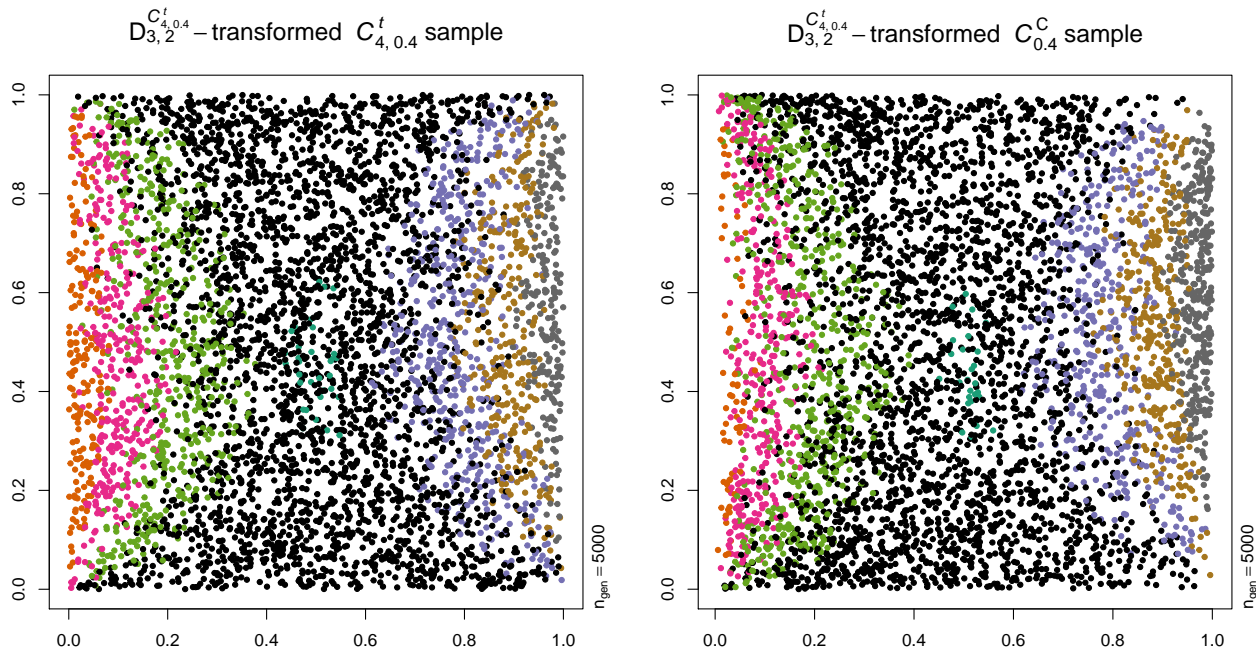


**Figure 3**  $D_{3,2}^{C_{4,0.4}^t}$ -transformed colored samples of size  $n_{\text{gen}} = 5000$  from trivariate  $C_{4,0.4}^t$  (left) and  $C_{0.4}^C$  (right) copulas.

example where the DecoupleNet maps from  $d$  to  $d'$  with  $3 = d > d' = 2$ , and we still see from the overrepresented dark color (joint left tail) and underrepresented bright color (joint right tail) which regions  $C_{0.4}^C$  fails to capture.

These examples already demonstrates how DecoupleNets can be utilized for graphical model assessment of copulas. For additional bivariate and higher-dimensional examples of graphical assessments in simulated and real-world settings, see Sections 3.1 and 4, respectively.

A question one may have is whether the trick with colors always works. For example, it would be much harder (or rather impossible) to interpret the under- or over-representation of colors if they were distributed all over the place (instead of within topologically connected regions) after the DecoupleNet transformation is applied. According to the following result based on the notion of topological connectedness, this cannot happen.

**Proposition 2.2 (Connected colored regions)**

A DecoupleNet maps connected colored regions to connected colored regions.

*Proof.* By Munkres (2000, Theorem 23.5), the image of a connected space under a continuous map is connected. The claim follows by realizing that DecoupleNets are continuous maps.  $\square$

Suppose we are given data  $\{\mathbf{X}_i\}_{i=1}^{n_{\text{trn}}}$  in  $\mathbb{R}^d$ , assumed to come from a joint distribution with continuous marginal distribution functions. Since our primary focus is on modeling the underlying dependence structure, we first compute the pseudo-observations  $\hat{U}_{i,j} = \hat{R}_{i,j}/(n_{\text{trn}}+1)$ ,  $i = 1, \dots, n_{\text{trn}}$ ,  $j = 1, \dots, d$ , where  $\hat{R}_{i,j}$  denotes the rank of  $X_{i,j}$  among  $X_{1,j}, \dots, X_{n_{\text{trn}},j}$ . Let  $\hat{C}_{n_{\text{trn}}}$  denote the

empirical copula of  $\{\hat{\mathbf{U}}_i\}_{i=1}^{n_{\text{trn}}}$ . Now suppose we are interested in selecting the best copula from a collection  $\mathcal{C}$  of candidate models. We denote an element of  $\mathcal{C}$  as  $C_{\boldsymbol{\theta}}$  for a parameter vector  $\boldsymbol{\theta}$ ; note however that  $C_{\boldsymbol{\theta}}$  could very well be a copula without any parameter vector to estimate, for example, if specified by an expert. For each parametric candidate model  $C_{\boldsymbol{\theta}} \in \mathcal{C}$ , we proceed by first fitting  $\boldsymbol{\theta}$  to the pseudo-observations  $\{\hat{\mathbf{U}}_i\}_{i=1}^{n_{\text{trn}}}$ . Next, we learn a DecoupleNet  $D_{d,d'}^{\hat{C}_{n_{\text{trn}}}}$  from the pseudo-observations  $\{\hat{\mathbf{U}}_i\}_{i=1}^{n_{\text{trn}}}$  to  $\text{U}(0,1)^{d'}$ . By passing samples from each fitted candidate copula  $C_{\hat{\boldsymbol{\theta}}}$  through  $D_{d,d'}^{\hat{C}_{n_{\text{trn}}}}$ , we can use the resulting DecoupleNet-transformed samples to rank the fit of the candidate copulas to the pseudo-observations, that is, the closer the DecoupleNet-transformed sample is to  $\text{U}(0,1)^{d'}$ , the better. Formulated as an algorithm, our proposed model selection procedure is summarized in Algorithm 2.3.

We can also numerically summarize how close a DecoupleNet output  $\{D_{d,d'}^C(\mathbf{U}_i)\}_{i=1}^{n_{\text{gen}}}$  is to  $\text{U}(0,1)^{d'}$  using a score of the Cramér-von-Mises (CvM) type,

$$S_{n_{\text{gen}},d'} = \int_{[0,1]^{d'}} n_{\text{gen}} \left( C_{n_{\text{gen}}}(\mathbf{u}) - \prod_{j=1}^{d'} u_j \right)^2 dC_{n_{\text{gen}}}(\mathbf{u}), \quad (4)$$

where  $C_{n_{\text{gen}}}$  is the empirical copula of the pseudo-observations of  $\{D_{d,d'}^C(\mathbf{U}_i)\}_{i=1}^{n_{\text{gen}}}$ , so the empirical copula of  $\{\mathbf{R}_i/(n_{\text{gen}} + 1)\}_{i=1}^{n_{\text{gen}}}$  with  $\mathbf{R}_i = (R_{i,1}, \dots, R_{i,d'})$ , where  $R_{i,j}$  denotes the rank of the  $j$ th among all components of  $D_{d,d'}^C(\mathbf{U}_i)$ .

The following algorithm describes both the graphical approach and the numerical summary of our proposed model selection procedure.

**Algorithm 2.3 (Model assessment and selection with DecoupleNets)**

- 1) Given data  $\{\mathbf{X}_i\}_{i=1}^{n_{\text{trn}}}$ , construct the pseudo-observations  $\{\hat{\mathbf{U}}_i\}_{i=1}^{n_{\text{trn}}}$ . Their empirical copula is denoted by  $\hat{C}_{n_{\text{trn}}}$ .
- 2) Train the DecoupleNet  $D_{d,d'}^{\hat{C}_{n_{\text{trn}}}}$  based on the pseudo-observations  $\{\hat{\mathbf{U}}_i\}_{i=1}^{n_{\text{trn}}}$  and the desired output  $\{\mathbf{U}'_i\}_{i=1}^{n_{\text{trn}}}$  from  $\text{U}(0,1)^{d'}$ .
- 3) For each parametric candidate copula  $C_{\boldsymbol{\theta}} \in \mathcal{C}$ , estimate the parameter  $\boldsymbol{\theta}$  of  $C_{\boldsymbol{\theta}}$  using the pseudo-observations  $\{\hat{\mathbf{U}}_i\}_{i=1}^{n_{\text{trn}}}$  to obtain  $C_{\hat{\boldsymbol{\theta}}}$ . This leaves us with a finite number of candidate copulas, fitted or fixed; the latter refers to copulas with fixed parameters where no estimation is necessary. We denote a generic candidate copula by  $\tilde{C}$ .
- 4) For each candidate copula  $\tilde{C}$  do:
  - 4.1) Generate a sample  $\{\tilde{\mathbf{U}}_i\}_{i=1}^{n_{\text{gen}}}$  from  $\tilde{C}$ .
  - 4.2) Pass  $\{\tilde{\mathbf{U}}_i\}_{i=1}^{n_{\text{gen}}}$  through the DecoupleNet  $D_{d,d'}^{\hat{C}_{n_{\text{trn}}}}$  to obtain  $\{D_{d,d'}^{\hat{C}_{n_{\text{trn}}}}(\tilde{\mathbf{U}}_i)\}_{i=1}^{n_{\text{gen}}}$ .
  - 4.3) For a graphical approach ( $d' = 2$ ), create a scatter plot of the DecoupleNet-transformed sample  $\{D_{d,d'}^{\hat{C}_{n_{\text{trn}}}}(\tilde{\mathbf{U}}_i)\}_{i=1}^{n_{\text{gen}}}$ . Determine the color of sample points  $\tilde{\mathbf{U}}_i$  according to regions of interest; then, color the sample  $\{D_{d,d'}^{\hat{C}_{n_{\text{trn}}}}(\tilde{\mathbf{U}}_i)\}_{i=1}^{n_{\text{gen}}}$  accordingly and create a colored scatter plot. For the numerical summary, compute the Cramér-von-Mises score  $S_{n_{\text{gen}},d'}$  of (4) for the DecoupleNet-transformed sample  $\{D_{d,d'}^{\hat{C}_{n_{\text{trn}}}}(\tilde{\mathbf{U}}_i)\}_{i=1}^{n_{\text{gen}}}$ .
- 5) For the graphical approach, compare the two types of scatter plots created in Step 4.3) for all candidate copulas  $\tilde{C}$  and select the candidate copula that shows least non-uniformity overall or in the region of interest. For the numerical summary, compare the Cramér-von-Mises scores for

all candidate copulas  $\tilde{C}$  and select the candidate copula that yields the lowest Cramér-von-Mises score.

In what follows we consider  $d' = 2$  which allows us to investigate both the graphical approach and the numerical summary for dependence model assessment and selection. We also investigated the numerical summary for  $d' > 2$  (results not presented) and found no advantage over  $d' = 2$ . Moreover, the case  $d' = 2$  has the advantage of reduced run time when training a DecoupleNet.

**Remark 2.4 (About the importance of graphical assessments)**

In many areas of statistics, graphical tools are preferred over summary statistics (single numbers); see, for example, the popularity of Q-Q plots for (univariate) model assessment. The problem with a numerical assessment through a summary statistic like (4) is that, if one deems a model not adequate based on a single number, one does not gain much information about *why* it is not adequate. As we mentioned in the beginning of Section 1, it is typically hard to find an adequate dependence model; most will be deemed inadequate. In these cases one needs to know *why* the model is inadequate and then make a decision about changing the model accordingly or whether to keep working with the model. In many applications, copula models are not necessarily used as overall models, but only in specific regions of interest. For example, if only the joint right tail is of interest, a copula model deemed overall inadequate but which provides a good fit in the joint right tail may very well be adequate to work with. As we have demonstrated in this section, graphical applications of DecoupleNets are useful for model assessment and selection based on regions of interest.

### 3 Model assessment and selection based on simulated data

In this section we investigate our model assessment and selection procedure based on simulated data. Section 3.1 considers the graphical approach, and Section 3.2 the numerical summary.

#### 3.1 Graphical approach

We first focus on the graphical assessment and selection approach. Figure 4 shows DecoupleNet-transformed samples from different copulas (columns) and from different dimensions (rows). Let us start by focusing on the first row. Here a DecoupleNet was trained on a sample of size  $n_{\text{trn}} = 50\,000$  from a bivariate  $C_{4,0.4}^t$  copula. The resulting DecoupleNet is  $D_{2,2}^{C_{4,0.4}^t}$ . Then samples of size  $n_{\text{gen}} = 5000$  from  $C_{4,0.4}^t$  (so the same copula as what the DecoupleNet was trained on, referred to as the *true* copula), from  $C_{4,0.2}^t$ ,  $C_{4,0.6}^t$  (so also  $t$  copulas with the same degrees of freedom but different Kendall’s tau), from  $C_{0.4}^F$  (the Archimedean Frank copula with Kendall’s tau 0.4) and from  $C_{0.4}^C$  copulas are generated and each is passed through the DecoupleNet  $D_{2,2}^{C_{4,0.4}^t}$  and then plotted in the first row of Figure 4 (from left to right). For the true copula, so the sample from  $C_{4,0.4}^t$ , the  $D_{2,2}^{C_{4,0.4}^t}$ -transformed samples look uniform as they should. And for all other candidate copulas, we clearly see non-uniformity in the  $D_{2,2}^{C_{4,0.4}^t}$ -transformed samples. The samples in the second and third row of Figure 4 are constructed similarly, using the same candidate copulas but now in  $d = 5$  (middle row) and  $d = 10$  (bottom row) dimensions; the corresponding DecoupleNets trained are denoted by  $D_{5,2}^{C_{4,0.4}^t}$  (middle row) and  $D_{10,2}^{C_{4,0.4}^t}$  (bottom row). We come to the same conclusion as in the first row – namely, that we correctly observe uniformity in the first column and non-uniformity in all others. From all plots showing departures from uniformity in Figure 4, we can even see that, across the dimensions  $d \in \{2, 5, 10\}$ , the type of non-uniformity remains roughly the same within

### 3 Model assessment and selection based on simulated data

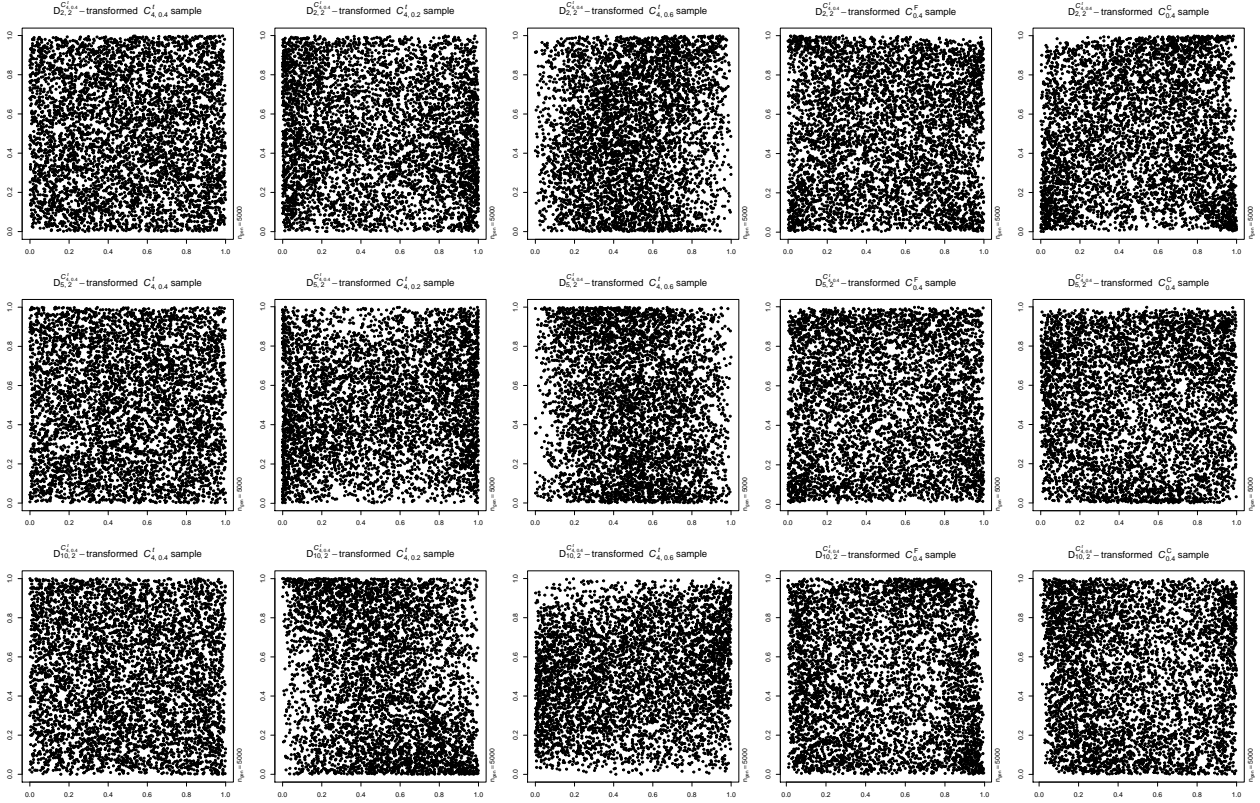


**Figure 4**  $D_{2,2}^{C_{4,0.4}^t}$ -transformed samples of size  $n_{\text{gen}} = 5000$  from bivariate  $C_{4,0.4}^t$ ,  $C_{4,0.2}^t$ ,  $C_{4,0.6}^t$ ,  $C_{0.4}^F$  and  $C_{0.4}^C$  copulas (top row, from left to right),  $D_{5,2}^{C_{4,0.4}^t}$ -transformed samples of the same size and from the same type of copulas but five-dimensional (middle row), and  $D_{10,2}^{C_{4,0.4}^t}$ -transformed samples of the same size and from the same type of copulas but ten-dimensional (bottom row).

### 3 Model assessment and selection based on simulated data

each column – up to rotation by a multiple of 90 degrees, an insignificant artifact stemming from the stochastic nature of our training procedure. This observation shows that we do not lose much information when mapping from  $d > 2$  to  $d' = 2$  for the purpose of model assessment and selection.

Next, Figure 5 shows the middle row of Figure 4 but with colored samples. As also in the rest of

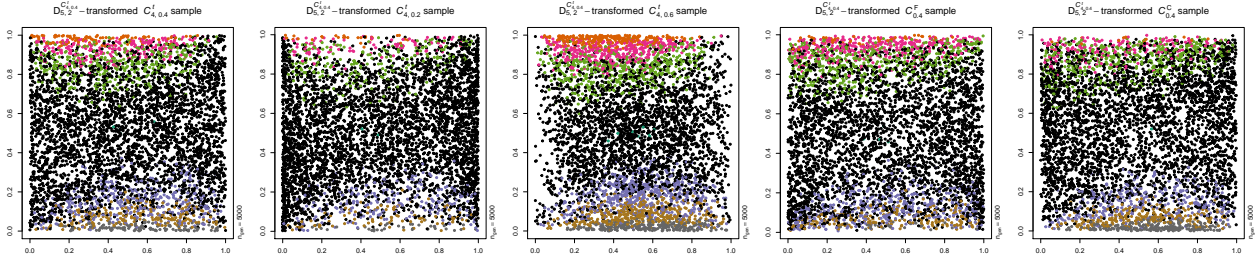


**Figure 5**  $D_{5,2}^{C_{4,0.4}^t}$ -transformed colored samples of size  $n_{\text{gen}} = 5000$  from five-dimensional  $C_{4,0.4}^t$ ,  $C_{4,0.2}^t$ ,  $C_{4,0.6}^t$ ,  $C_{0.4}^F$  and  $C_{0.4}^C$  copulas (from left to right). The plots correspond to the middle row of Figure 4 but with colors.

the paper, we used the same color scheme here as we have already seen in Figure 2, so darker colors correspond to the joint left tail and brighter colors to the joint right tail of the input sample or copula. This allows us to assess the different five-dimensional candidate copulas, and ultimately to select one of them, according to their ability to properly capture, say, the joint right tail. For example, the  $D_{5,2}^{C_{4,0.4}^t}$ -transformed samples from  $C_{4,0.2}^t$  (second plot) and  $C_{0.4}^C$  (last plot) show too few bright points in the top region and thus underestimate the joint right tail; this can also be verified numerically, the probability to fall in  $[6/7, 1]^5$  is about 0.0673 under  $C_{4,0.4}^t$  but only 0.0457 under  $C_{4,0.2}^t$  and 0.0400 under  $C_{0.4}^C$ . Similarly, the  $D_{5,2}^{C_{4,0.4}^t}$ -transformed sample from  $C_{4,0.6}^t$  (third plot) shows too many points in the top region and thus overestimates the joint right tail; the probability to fall in  $[6/7, 1]^5$  is about 0.0912 under  $C_{4,0.6}^t$ . Selecting a model based on only the joint right tail region (an important region for risk management applications, for example), we select  $C_{0.4}^F$  (fourth plot); again this can be confirmed numerically, the probability to fall in  $[6/7, 1]^5$  under  $C_{0.4}^F$  is 0.0548, which is closest to the probability 0.0673 of the true model among all other candidate models.

In our next example we consider deviations from the true  $t$  copula in some entries of the underlying correlation matrix  $P$ . To this end we use trivariate  $t$  copulas with  $\nu = 4$  degrees of freedom and correlation matrices  $P$  of hierarchical nature. The top row of Figure 6 shows scatter plot matrices of the trivariate samples with size  $n_{\text{gen}} = 5000$  from these models, denoted by  $C_{4,(0.2,0.7)}^t$ ,  $C_{4,(0.4,0.7)}^t$  and  $C_{4,0.45}^t$  (from left to right). The notation for the former two models is  $C_{4,(\tau_0,\tau_1)}^t$ , where  $\tau_0$  is the Kendall's tau corresponding to the entries  $\rho_{13}, \rho_{23}$  or the correlation matrix  $P$  of the  $t$  copula, whereas  $\tau_1$  corresponds to the entry  $\rho_{12}$  of  $P$ ; note that for  $t$  copulas, one has  $\rho = \sin(\tau\pi/2)$ . The bottom row of Figure 6 shows scatter plots of the  $D_{3,2}^{C_{4,(0.2,0.7)}^t}$ -transformed samples of  $C_{4,(0.2,0.7)}^t$  (the true copula here),  $C_{4,(0.4,0.7)}^t$  (deviating in  $\tau_0$ , so in  $\rho_{13}, \rho_{23}$ ) and  $C_{4,0.45}^t$  (deviating in all entries of  $P$  but capturing the average Kendall's tau  $(0.2 + 0.7)/2$ ). As before, also here we correctly see uniformity in the first, and non-uniformity in the other two plots.

### 3.2 Numerical summary

Despite the drawbacks of using just a numerical summary for model assessment and selection (Remark 2.4), in this section we still investigate it further, largely because it is much easier to

### 3 Model assessment and selection based on simulated data

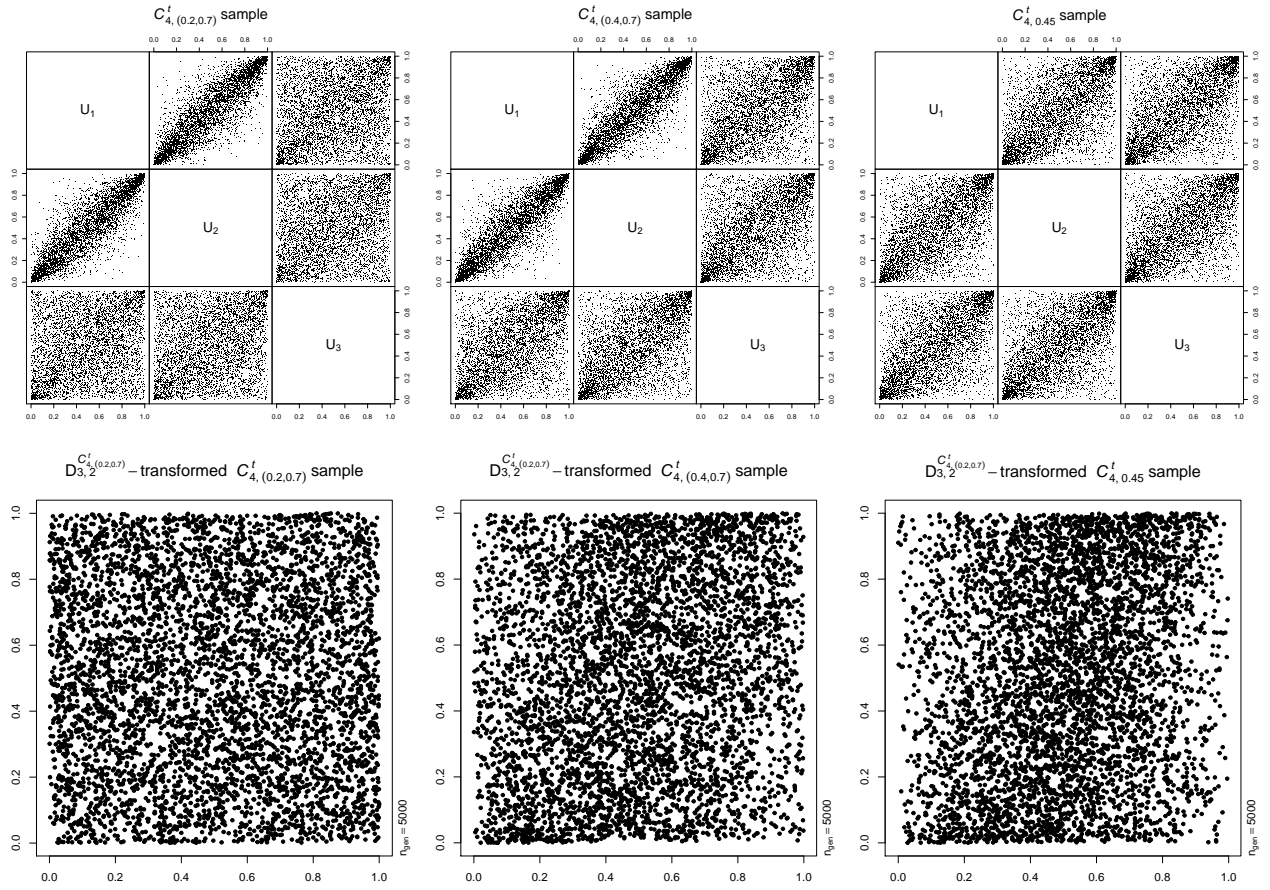


**Figure 6** Samples of size  $n_{\text{gen}} = 5000$  from trivariate  $C_{4,(0.2,0.7)}^t$ ,  $C_{4,(0.4,0.7)}^t$  and  $C_{4,0.45}^t$  copulas (top row, from left to right), with corresponding  $D_{3,2}^{C_4^t(0.2,0.7)}$ -transformed samples (bottom row).

report replications for single numeric summaries than it is for graphical assessments. The following algorithm summarizes what we do in this section for various dependence models to be specified later.

**Algorithm 3.1 (Numerical model assessment and selection based on simulated data)**

- 1) Fix a  $d$ -dimensional copula  $C$  and a number  $B \in \mathbb{N}$  of replications.
- 2) For  $b = 1, \dots, B$  do:
  - 2.1) Generate a sample of size  $n_{\text{trn}}$  from  $C$  and compute its pseudo-observations  $\{\hat{\mathbf{U}}_i^{(b)}\}_{i=1}^{n_{\text{trn}}}$ ; we use pseudo-observations here to mimic a realistic scenario as would be the case for real world data.
  - 2.2) Train the DecoupleNet  $D_{d,2}^C$  on the pseudo-observations  $\{\hat{\mathbf{U}}_i^{(b)}\}_{i=1}^{n_{\text{trn}}}$ .
  - 2.3) For the true copula  $C$  and each candidate copula  $\tilde{C}$ , do:
    - 2.3.1) If the copula contains unknown parameters, estimate them using the pseudo-observations  $\{\hat{\mathbf{U}}_i^{(b)}\}_{i=1}^{n_{\text{trn}}}$ .
    - 2.3.2) Generate a sample  $\{\tilde{\mathbf{U}}_i\}_{i=1}^{n_{\text{gen}}}$  of size  $n_{\text{gen}}$  from the (fitted) copula.
    - 2.3.3) Pass  $\{\tilde{\mathbf{U}}_i\}_{i=1}^{n_{\text{gen}}}$  through the trained DecoupleNet  $D_{d,2}^C$  and obtained the decoupled output sample.
    - 2.3.4) Evaluate the decoupled output sample by computing the CvM score (4).
- 3) Create box plots of the computed CvM scores.

Where applicable, we also include a comparison with Rosenblatt-transformed data and box plots of sliced Wasserstein distances (introduced below).

We apply Algorithm 3.1 in three settings. In all three we consider  $d \in \{3, 5, 10\}$ ,  $B = 25$ ,  $n_{\text{trn}} = 50\,000$  and  $n_{\text{gen}} = 10\,000$ . In the first and third setting, the copulas were chosen among the few with analytically available Rosenblatt transform to allow for a comparison.

In the first setting, we consider  $C_{0.4}^C$  as true copula  $C$  in Algorithm 3.1, and  $C_{0.4}^F$ ,  $C_{4,0.4}^t$ ,  $C_{0.2}^C$  and  $C_{0.6}^C$  as candidate copulas. The left-hand side of Figure 7 shows box plots of the CvM scores according to Algorithm 3.1 for  $d = 3$  (top),  $d = 5$  (middle) and  $d = 10$  (bottom). The middle includes similar plots but obtained from applying the Rosenblatt transform  $R_d^{C_{0.4}^C}$  instead of a DecoupleNet  $D_{d,2}^{C_{0.4}^C}$ . In particular, recall that the Rosenblatt transform maps to  $d' = d > 2$  dimensions so the values of the CvM scores are not directly comparable. Nevertheless, apart from  $C_{4,0.4}^t$  (for  $d \in \{3, 5\}$ ) and  $C_{0.2}^C$  (for  $d = 10$ ), the rankings of the candidate models are the same. A comparison with the box plot of the true copula  $C_{0.4}^C$  also correctly reveals that based on both  $D_{d,2}^{C_{0.4}^C}$  and  $R_d^{C_{0.4}^C}$ , none of the candidate copulas is adequate. Finally, the right column of plots in Figure 7 shows box plots of the sliced Wasserstein score  $SW_{n_{\text{trn}}, n_{\text{gen}}}$ ; see Bonneel et al. (2015). This score is computed between the training samples  $\hat{U} = \{\hat{\mathbf{U}}_i\}_{i=1}^{n_{\text{trn}}}$  and generated samples  $\tilde{U} = \{\tilde{\mathbf{U}}_i\}_{i=1}^{n_{\text{gen}}}$  from the aforementioned (true or candidate) copulas via

$$SW_{n_{\text{trn}}, n_{\text{gen}}} = \left( \frac{1}{n_{\text{prj}}} \sum_{i=1}^{n_{\text{prj}}} \sum_{k=1}^m \left| \hat{F}_{\hat{U}\mathbf{P}_i, m}^{-1} \left( \frac{k-1/2}{m} \right) - \hat{F}_{\tilde{U}\mathbf{P}_i, m}^{-1} \left( \frac{k-1/2}{m} \right) \right|^p \right)^{1/p},$$

where  $\mathbf{P}_i = \mathbf{Z}_i / \|\mathbf{Z}_i\|_2$  for  $\mathbf{Z}_i \stackrel{\text{ind.}}{\sim} \mathcal{N}_d(\mathbf{0}, I_d)$ ,  $i = 1, \dots, n_{\text{prj}} = 1000$ , are random projections,  $\hat{U}\mathbf{P}_i$  (respectively  $\tilde{U}\mathbf{P}_i$ ) denotes the univariate dataset with empirical quantile function  $\hat{F}_{\hat{U}\mathbf{P}_i, m}^{-1}$  (respectively

### 3 Model assessment and selection based on simulated data

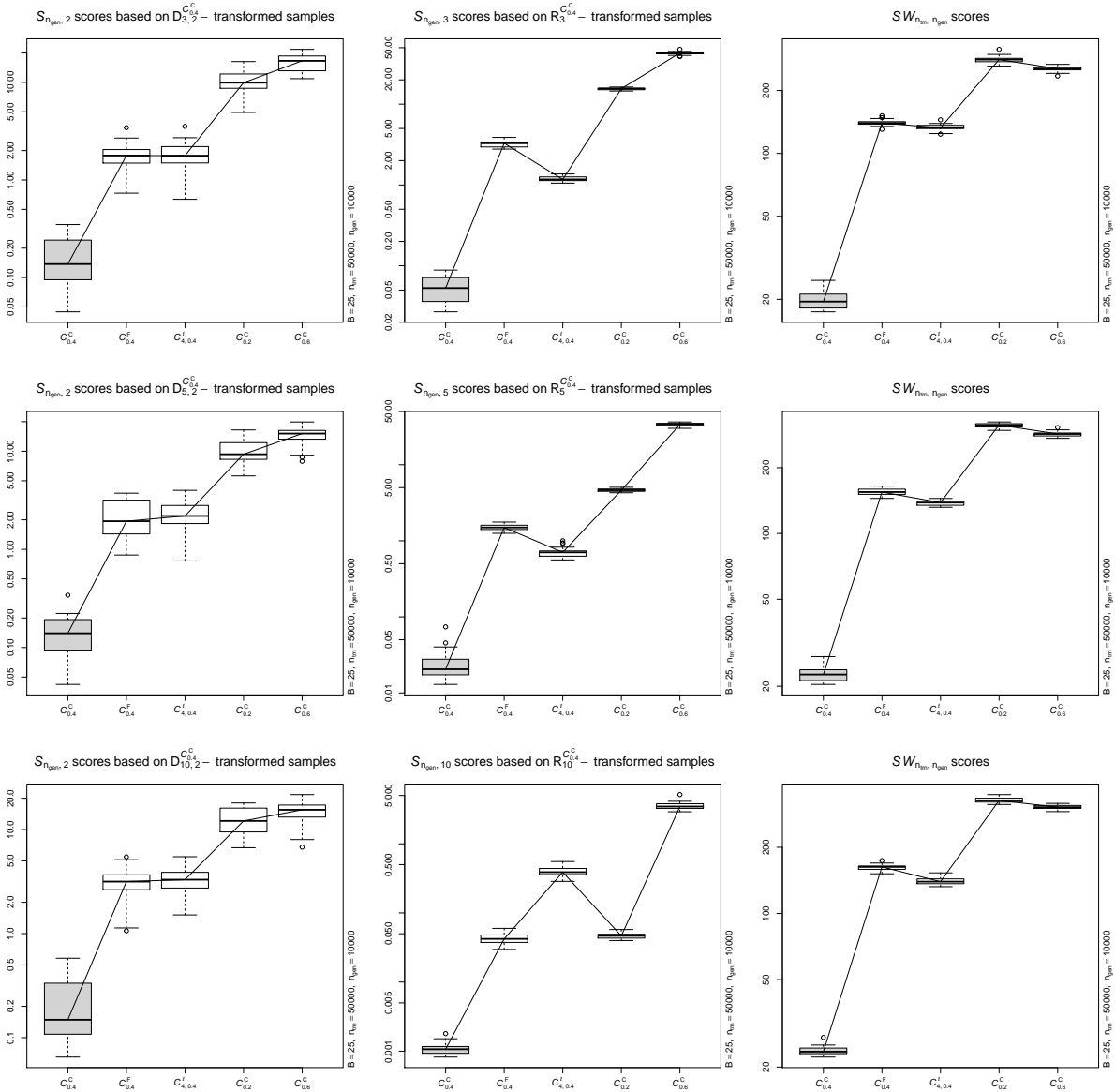


**Figure 7** The left column shows box plots of CvM scores  $S_{n_{gen},2}$  based on  $B = 25 D_{d,2}^{C^C}$ -transformed samples of size  $n_{gen} = 10000$  from trivariate ( $d = 3$ ; top), five-dimensional ( $d = 5$ ; middle) and ten-dimensional ( $d = 10$ ; bottom) copulas  $C_{0.4}^C$ ,  $C_{0.4}^F$ ,  $C_{4,0.4}^t$ ,  $C_{0.2}^C$  and  $C_{0.6}^C$ ; see Algorithm 3.1 for details. The middle column shows the same for  $R_d^{C^C}$ -transformed samples. The right column shows box plots of sliced Wasserstein scores  $SW_{n_{trn}, n_{gen}}$ , computed between the training samples and generated samples from the aforementioned copulas.

$\hat{F}_{\tilde{U}_{\mathbf{P}_i, m}}^{-1}$ ) resulting from projecting  $U$  (respectively  $\tilde{U}$ ) onto  $\mathbf{P}_i$ , and  $m = \min\{n_{\text{trn}}, n_{\text{gen}}\}$ . We can see that the ranking according to this metric (computed without transforming samples to multivariate uniformity first) is mostly in line with the previous rankings.

In the second setting, we consider nested Clayton copulas as true copula  $C$  in Algorithm 3.1. To this end let  $C_k$ ,  $k = 0, 1, 2$ , be a Clayton copula with parameter chosen such that Kendall's tau equals  $\tau_k$ . For  $d = 3$  we choose a (2, 1)-nested Clayton copula  $C_0(C_1(u_1, u_2), u_3)$  with  $(\tau_0, \tau_1) = (0.2, 0.4)$ , denoted by  $C_{(0.2, 0.4)}^C$ . Besides this copula as true copula, we consider the trivariate candidate models  $C_{(0.2, 0.5)}^C$ ,  $C_{(0.3, 0.4)}^C$ ,  $C_{0.27}^C$  and  $C_{4, 0.27}^t$ . The top left plot of Figure 8 shows the box plots of the CvM scores according to Algorithm 3.1. For  $d = 5$  we choose a (2, 3)-nested Clayton copula  $C_0(C_1(u_1, u_2), C_2(u_3, u_4, u_5))$  with  $(\tau_0, \tau_1, \tau_2) = (0.2, 0.4, 0.6)$ , denoted by  $C_{(0.2, 0.4, 0.6)}^C$ . Besides this copula as true copula, we consider the five-dimensional candidate models  $C_{(0.2, 0.5, 0.75)}^C$ ,  $C_{(0.3, 0.4, 0.6)}^C$ ,  $C_{0.34}^C$  and  $C_{4, 0.34}^t$ . The resulting box plots of the CvM scores according to Algorithm 3.1 are shown in the middle left of Figure 8. And for  $d = 10$  we choose a (5, 5)-nested Clayton copula  $C_0(C_1(u_1, \dots, u_5), C_2(u_6, \dots, u_{10}))$  with  $(\tau_0, \tau_1, \tau_2) = (0.2, 0.4, 0.6)$ , also denoted by  $C_{(0.2, 0.4, 0.6)}^C$ , and ten-dimensional candidate models  $C_{(0.2, 0.5, 0.75)}^C$ ,  $C_{(0.3, 0.4, 0.6)}^C$ ,  $C_{0.33}^C$  and  $C_{4, 0.33}^t$ . The resulting box plots of the CvM scores are shown in the bottom left of Figure 8. Among the candidate models, the first two are also of hierarchical nature, just with different parameters, whereas the other candidate models are exchangeable with parameters chosen to match the average pairwise dependence. That is, for  $d = 3$ ,  $d = 5$  and  $d = 10$  copulas, we set  $\tau = \frac{1}{3}(2\tau_0 + \tau_1)$ ,  $\tau = \frac{1}{5}(6\tau_0 + \tau_1 + 3\tau_2)$  and  $\tau = \frac{1}{10}(25\tau_0 + 10\tau_1 + 10\tau_2)$ , respectively. As results, we clearly see from Figure 8 that none of the exchangeable or nested candidate models are adequate, which aligns with intuition. Moreover, from the rankings of the two nested models, we see that the deviation in  $\tau_0$  is more important than deviations in both  $\tau_1$  or  $\tau_2$ . This is due to the fact that there exist more pairwise marginal copula with Kendall's tau  $\tau_0$  than those with Kendall's tau  $\tau_1$  and Kendall's tau  $\tau_2$  combined. The right column of Figure 8 shows the corresponding box plots of the sliced Wasserstein score; again, the ranking according to this metric is mostly in line with those obtained via the DecoupleNet transformed samples.

In the third and final setting, we consider an unstructured  $t$  copula with  $\nu = 4$  degrees of freedom and random correlation matrix as true copula, in  $d = 3$ ,  $d = 5$  and  $d = 10$  dimensions. As benchmark we include a fitted (unstructured)  $t$  copula  $\hat{C}_{\text{un}}^t$ . As candidate copulas we include a fitted vine copula  $\hat{C}^V$  (fitted with `RvineStructureSelect()` from the R package `VineCopula` with tree structure selected using Dissman's algorithm in Dissmann et al. (2013) and AIC to select the pair-copula families), a fitted unstructured normal copula  $\hat{C}_{\text{un}}^N$ , a fitted exchangeable normal copula  $\hat{C}_{\text{ex}}^N$  and a fitted Frank copula  $\hat{C}^F$ . The left-hand column of Figure 9 shows the box plots of the CvM scores according to Algorithm 3.1 for  $d = 3$  (top),  $d = 5$  (middle) and  $d = 10$  (bottom). The center column includes similar plots but obtained from applying the Rosenblatt transform  $R_d^{C_{d, 2}^t, \text{un}}$  instead of a DecoupleNet  $D_{d, 2}^{C_{d, 2}^t, \text{un}}$ . And the right column contains the box plots based on the sliced Wasserstein score. We observe here that the rankings produced from these different scores are fairly comparable as well. In particular, the sliced Wasserstein score (again, not involving a transformation to uniformity first) does not do a better job at distinguishing  $\hat{C}^V$  from  $\hat{C}_{\text{un}}^t$ ; note that the slightly larger variance for the  $D_{d, 2}^{C_{d, 2}^t, \text{un}}$ -transformed samples does not come as a surprise due to the retraining of the DecoupleNet  $B$  times, a price one has to pay for the gain in flexibility.

### 3 Model assessment and selection based on simulated data

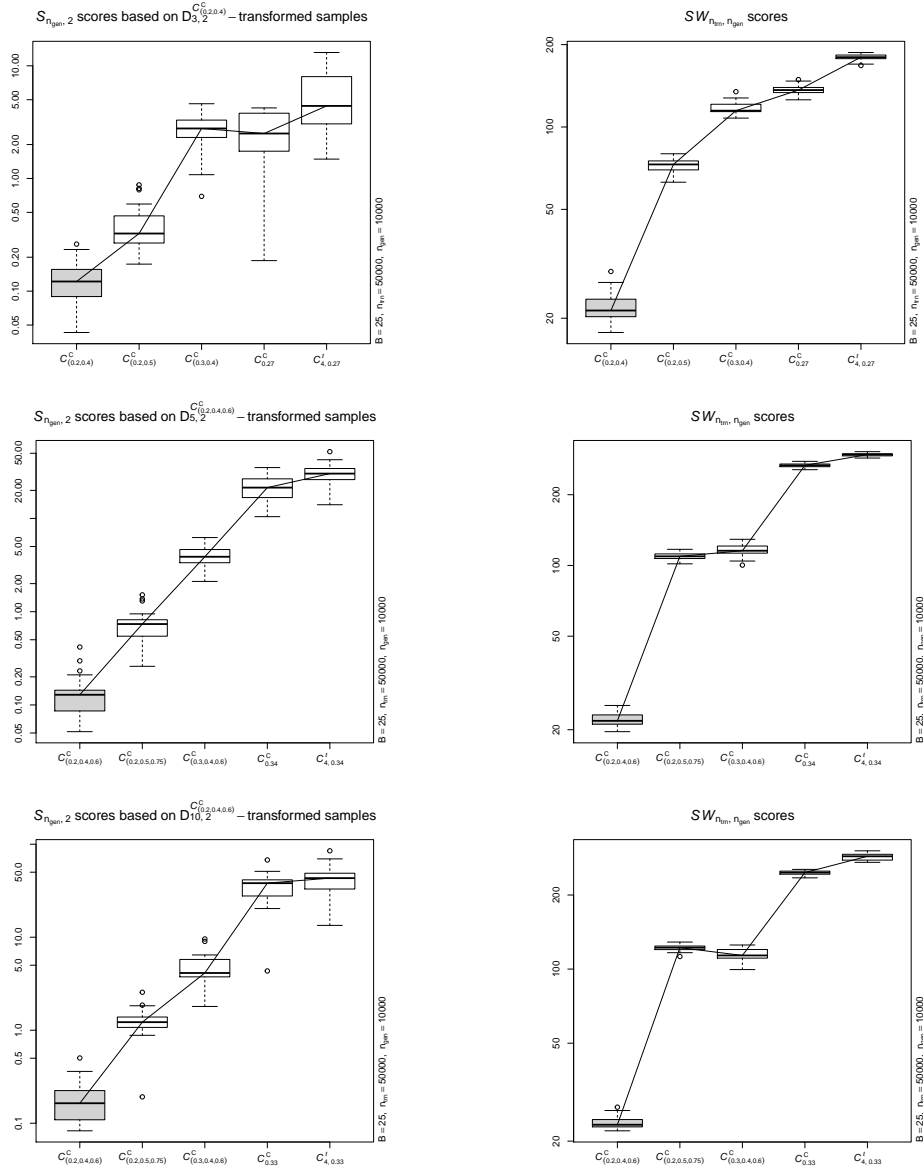


**Figure 8** The left column shows box plots of CvM scores  $S_{n_{gen},2}$  based on  $n_{rep} = 25$   $D_{3,2}^{C_{(0.2,0.4)}^C}$ -transformed samples of size  $n_{gen} = 10000$  from trivariate copulas  $C_{(0.2,0.4)}^C$ ,  $C_{(0.2,0.5)}^C$ ,  $C_{(0.3,0.4)}^C$ ,  $C_{0.27}^C$ ,  $C_{4,0.27}^C$  (top);  $D_{5,2}^{C_{(0.2,0.4,0.6)}^C}$ -transformed samples of the same size from five-dimensional copulas  $C_{(0.2,0.4,0.6)}^C$ ,  $C_{(0.2,0.5,0.75)}^C$ ,  $C_{(0.3,0.4,0.6)}^C$ ,  $C_{0.34}^C$ ,  $C_{4,0.34}^C$  (middle); and  $D_{10,2}^{C_{(0.2,0.4,0.6)}^C}$ -transformed samples of the same size from ten-dimensional copulas  $C_{(0.2,0.4,0.6)}^C$ ,  $C_{(0.2,0.5,0.75)}^C$ ,  $C_{(0.3,0.4,0.6)}^C$ ,  $C_{0.33}^C$ ,  $C_{4,0.33}^C$  (bottom); see Algorithm 3.1 for details. The right column shows box plots of sliced Wasserstein scores  $SW_{n_{trn}, n_{gen}}$ , computed between the training samples and generated samples from the aforementioned copulas.

### 3 Model assessment and selection based on simulated data

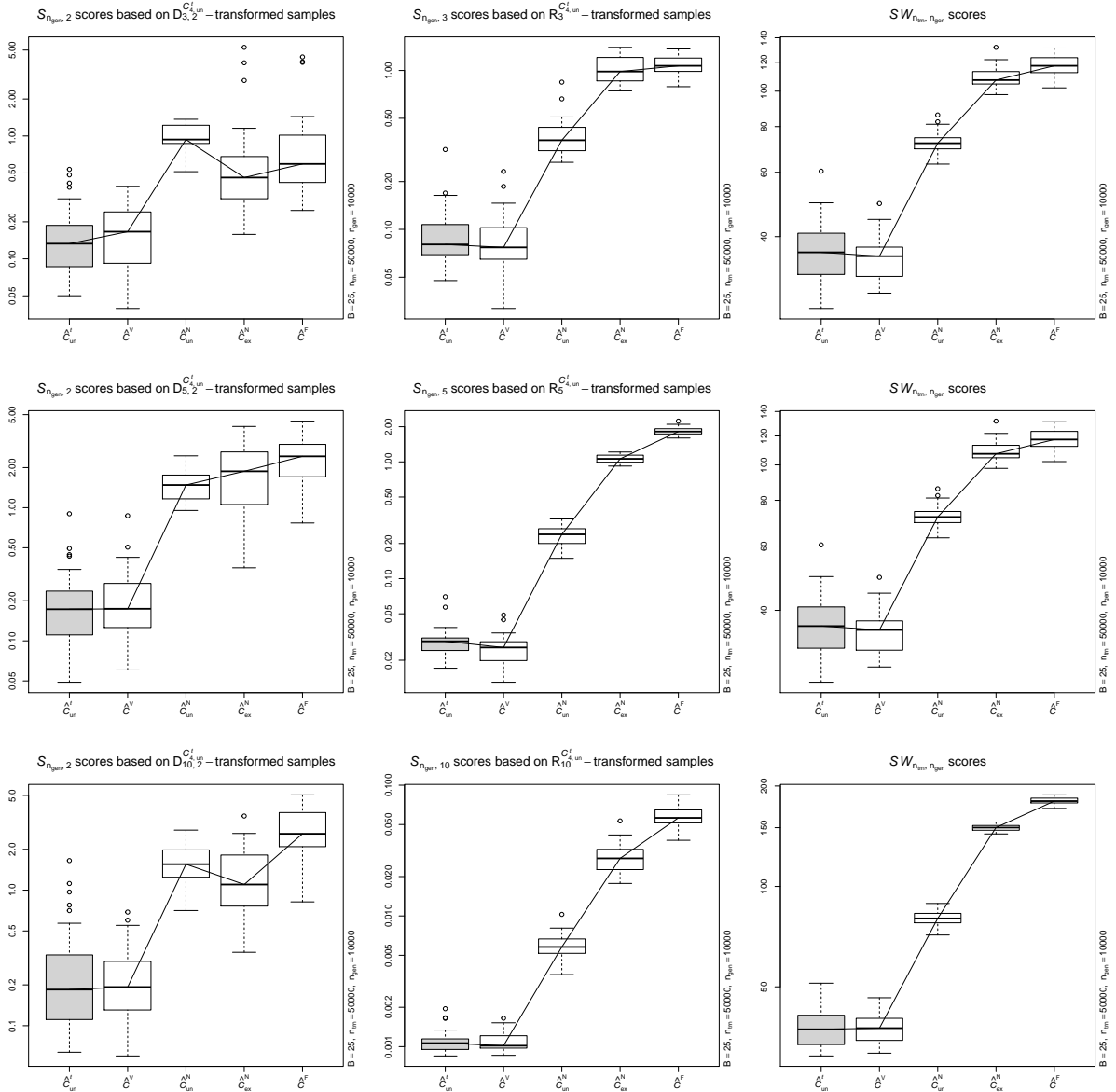


**Figure 9** The left column shows box plots of CvM scores  $S_{n_{\text{gen}},2}$  based on  $B = 25 D_{d,2}^{C_{4,\text{un}}^t}$ -transformed samples of size  $n_{\text{gen}} = 10\,000$  from trivariate ( $d = 3$ ; top), five-dimensional ( $d = 5$ ; middle) and ten-dimensional ( $d = 10$ ; bottom) fitted copulas  $\hat{C}_{\text{un}}^t$ ,  $\hat{C}^V$ ,  $\hat{C}_{\text{un}}^N$ ,  $\hat{C}_{\text{ex}}^N$  and  $\hat{C}^F$ ; see Algorithm 3.1 for details. The middle column shows the same for  $R_d^{C_{4,\text{un}}^t}$ -transformed samples. The right column shows box plots of sliced Wasserstein scores  $SW_{n_{\text{trn}},n_{\text{gen}}}$ , computed between the training samples and generated samples from the aforementioned copulas.

## 4 Model assessment and selection based on real world data

In this section we apply our DecoupleNet approach to two real world datasets. The first contains pseudo-observations of the water-level heights of two rivers; the second consists of two sets of foreign exchange rates.

### 4.1 Danube data

We consider the dataset `danube` from the R package `lcopula`, referred to as the “Danube data” in what follows. It consists of 659 pseudo-observations of prewhitened monthly average water-level heights of the Danube river at Nagyramos (Hungary) and those of the Inn river at Schärding (Austria); for more information about the Danube data, including the type of prewhitening applied, see the help page of `danube` in `lcopula`. With the Inn being a tributary to the Danube, the two water-level heights are naturally dependent, and Hofert, Kojadinovic, et al. (2018, Section 5.2.5) showed that there is no strong evidence against the hypothesis that this dependence is Gumbel.

For demonstrating our graphical assessment and selection procedure, we train a DecoupleNet  $D_{2,2}^{\hat{C}_n}$  on the Danube data. We then pass  $n_{\text{gen}} = 659$  samples from various copulas through  $D_{d,2}^{\hat{C}_n}$ . As benchmark, we include  $\hat{C}_n$ ; sampling from  $\hat{C}_n$  is done in the usual way, by drawing pseudo-observations at random with replacement. As candidate models, we include a Gumbel copula, a normal copula, a  $t$  copula, a Clayton copula and the independence copula. All parameters of the candidate models were estimated from the Danube data. The top row of Figure 10 shows scatter plots of the  $D_{d,2}^{\hat{C}_n}$ -transformed samples for the Danube data, and the bottom row shows the samples colored with the same color scheme as before, so, for example, samples with bright colors are decoupled samples from the joint right tail of the input sample. The graphical assessment and

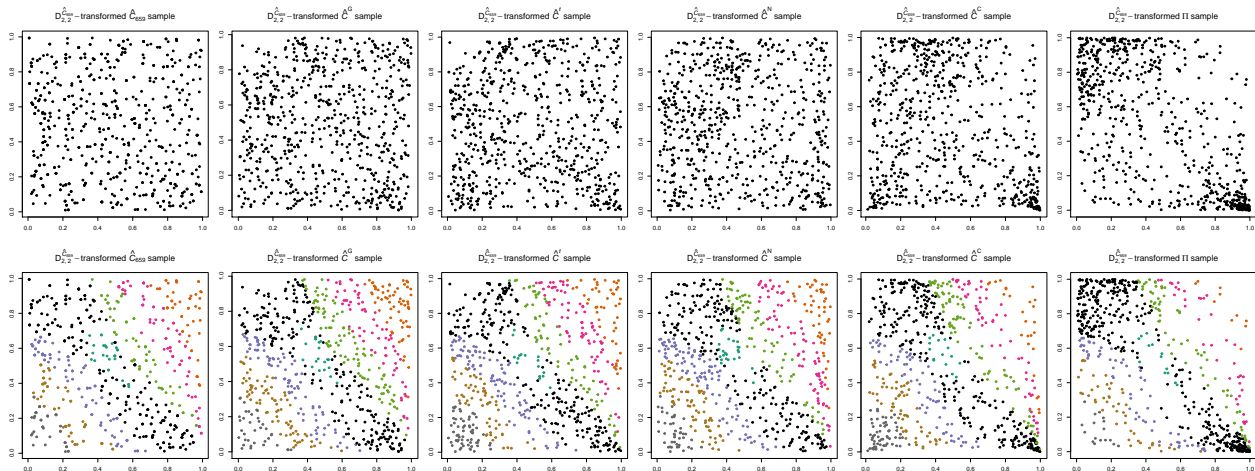


**Figure 10**  $D_{2,2}^{\hat{C}_n}$ -transformed samples of size  $n_{\text{gen}} = 659$  from the bivariate empirical copula  $\hat{C}_n$  of the Danube data for  $n = 659$ , a fitted Gumbel,  $t$ , normal, Clayton and the independence copula (top row, from left to right), and the same samples with colors (bottom row).

selection procedure is a bit more challenging to apply in this case due to the small sample size  $n = 659$  of the dataset. We cannot select a clear winner among the fitted Gumbel,  $t$  or normal copulas. Nevertheless, we see (more) non-uniformity for the fitted Clayton and the independence copula. Similarly for the corresponding colored plots in the bottom row of Figure 10.

We can additionally compare the numerical summary for the same set of models. For each one,

we generate  $n_{\text{rep}} = 25$  samples of size  $n_{\text{gen}} = 10\,000$  and pass them through the DecoupleNet  $D_{2,2}^{\hat{C}_n}$ . We then compute the corresponding CvM scores  $S_{n_{\text{gen}},2}$ ; see (4). The resulting box plots are shown in Figure 11. The numerical summaries based on the CvM scores here indeed reveal the fitted

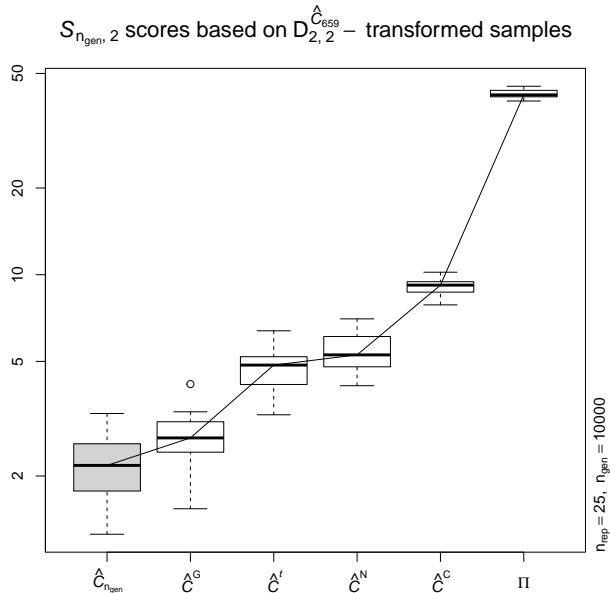


**Figure 11** Box plots of CvM scores  $S_{n_{\text{gen}},2}$  based on  $n_{\text{rep}} = 25$   $D_{2,2}^{\hat{C}_n}$ -transformed samples of size  $n_{\text{gen}} = 10\,000$  from bivariate copulas  $\hat{C}_{n_{\text{gen}}}$ ,  $\hat{C}^G$ ,  $\hat{C}^t$ ,  $\hat{C}^N$ ,  $\hat{C}^C$  fitted to the Danube data with sample size  $n = 659$ . Also included is the independence copula  $\Pi$ . See Algorithm 2.3 for details.

Gumbel copula as an adequate dependence model and best among all candidate copulas.

## 4.2 Exchange rate data

Here we consider two datasets of foreign exchange rates (FX) with the goal of investigating the dependence for each of these datasets, an important task from the realm of risk management. The data can be found in the R package `qrmdata`. The first dataset consists of daily exchange rates of Canadian dollar (CAD), Pound sterling (GBP), Euro (EUR), Swiss Franc (CHF) and Japanese yen (JPY) with respect to the US dollar (USD). And the second consists of daily exchange rates of CAD, USD, EUR, CHF, JPY and the Chinese Yuan (CNY) with respect to the GBP. The considered trading days are from 2000-01-01 to 2015-12-31, resulting in 5844 five-dimensional ( $d = 5$ ) and six-dimensional ( $d = 6$ ) observations for the USD and the GBP FX datasets, respectively. For each of the two datasets, negative log-returns were formed and deGARCHed; see Hofert, Prasad, et al. (2021a) for more details. This leaves us with  $n = 5843$  observations per dataset.

For demonstrating our graphical assessment and selection procedure, we consider the pseudo-observations with corresponding  $d$ -dimensional empirical copula  $\hat{C}_n$  for both datasets. For each dataset, we trained a DecoupleNet  $D_{d,2}^{\hat{C}_n}$  on these pseudo-observations. We then pass  $n_{\text{gen}} = 5000$  samples from various copulas through  $D_{d,2}^{\hat{C}_n}$ . As benchmark, we include  $\hat{C}_n$ . And as candidate models, we include a vine copula, a  $t$  copula with unstructured correlation matrix, an exchangeable normal copula with homogeneous correlation matrix, a Clayton copula and the independence copula. All parameters of the candidate models were estimated from the respective pseudo-observations.

#### 4 Model assessment and selection based on real world data

The first row of Figure 12 shows scatter plots of the  $D_{d,2}^{\hat{C}_n}$ -transformed samples for the USD FX data ( $d = 5$ ), and the second row shows the samples colored with the same color scheme as before. Rows three and four of Figure 12 show similar plots as rows one and two, respectively, but now

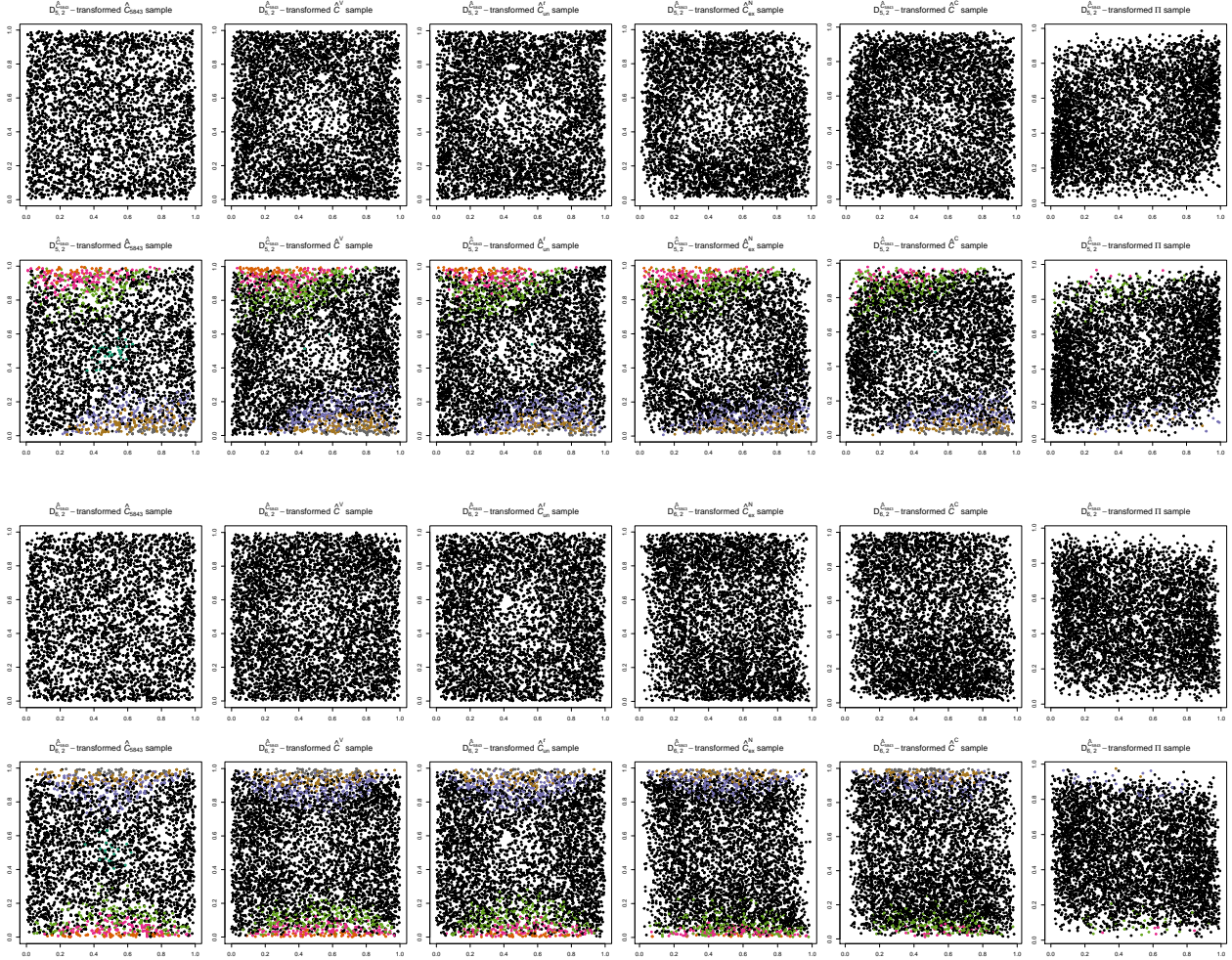


**Figure 12** First row:  $D_{d,2}^{\hat{C}_n}$ -transformed samples of size  $n_{\text{gen}} = 5000$  from the  $d$ -dimensional (with  $d = 5$ ) empirical copula  $\hat{C}_n$  of the FX USD data for  $n = 5843$ , a fitted vine, unstructured  $t$ , exchangeable normal, Clayton and the independence copula (from left to right). Second row: the same samples with colors. Third and fourth rows: same as first two rows, but now for the  $d$ -dimensional (with  $d = 6$ ) GBP FX data. The parameters of the candidate copulas in the center four columns were estimated.

for the GBP FX data ( $d = 6$ ). The first column shows uniformity of the DecoupleNet-transformed samples of the empirical copula  $\hat{C}_n$ , so training of the two DecoupleNets worked well. The samples corresponding to all candidate models show non-uniformity, though, so none of them seems to fit the respective dataset well, supporting our statement in the first paragraph of Section 1. From the (barely visible) mid-range colored samples in row two and four, we can identify that none of the candidate models fits well in the body of the underlying  $d$ -dimensional distribution. Judging from the fits in the joint right tail (bright colors), both the fitted vine and the fitted  $t$  copulas seem adequate for capturing the dependence in this region.

We can also compare the numerical summary for all candidate models as per Section 3.2. For

## 5 Conclusion

each of the datasets and models considered, we generate  $n_{\text{rep}} = 25$  samples of size  $n_{\text{gen}} = 10000$  and pass them through the respective DecoupleNet  $D_{5,2}^{\hat{C}_n}$  (for the USD FX data) or  $D_{6,2}^{\hat{C}_n}$  (for the GBP FX data). We then compute the corresponding CvM scores  $S_{n_{\text{gen}},2}$ ; see (4). The resulting box plots are shown in Figure 13. Our conclusion from the numerical summary is the same as from the

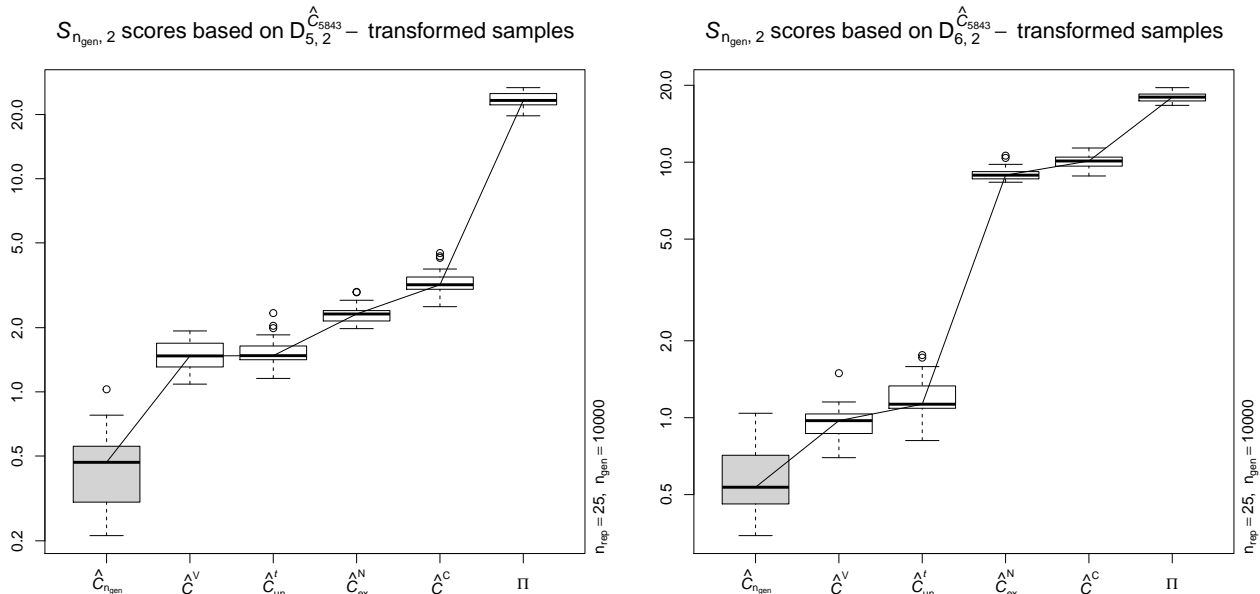


**Figure 13** Box plots of CvM scores  $S_{n_{\text{gen}},2}$  based on  $n_{\text{rep}} = 25$   $D_{d,2}^{\hat{C}_n}$ -transformed samples of size  $n_{\text{gen}} = 10000$  from  $d$ -dimensional copulas  $\hat{C}_{n_{\text{gen}}}$ ,  $\hat{C}^V$ ,  $\hat{C}_{\text{un}}^t$ ,  $\hat{C}_{\text{ex}}^N$ ,  $\hat{C}^C$  fitted to the FX USD data for  $d = 5$  (left) and the FX GBP data for  $d = 6$  (right) with sample size  $n = 5843$ . Also included is the independence copula  $\Pi$ . See Algorithm 2.3 for details.

graphical approach. We see from the box plots that none of the candidate models are particularly good for the respective data set, with vine and  $t$  copulas performing best on both the USD and the GBP FX data.

## 5 Conclusion

We introduced DecoupleNets for dependence model assessment and selection. A DecoupleNet is a neural network based transformation of a random vector from a copula to a random vector from a standard uniform distribution. A DecoupleNet can be trained on samples from a known copula or, more importantly, on pseudo-observations from a given multivariate dataset for which no copula is known. A candidate copula for the given dataset can then be assessed by computing a DecoupleNet-transformed sample from the candidate model and assessing its (non-)uniformity. Model selection can be done by comparing the (non-)uniformity of DecoupleNet-transformed samples from the candidate models and selecting the one producing the least non-uniform output. For both tasks, the flexibility of neural networks is a main advantage and allows DecoupleNets to be trained on and applied to any copula sample. Another advantage is that DecoupleNets can map to the (bivariate) unit square, which is computationally advantageous and, especially, allows for a graphical approach to assess and select dependence models. In particular, coloring input samples and corresponding DecoupleNet-transformed output samples even allows one to assess and select dependence models based on particular regions of interest, a fact particularly important for practical

applications in which dependence models often turn out to be inadequate as models overall, but are only of interest in specific regions such as the tails.

## References

- Bonneel, N., Rabin, J., Peyré, G., and Pfister, H. (2015), Sliced and Radon Wasserstein Barycenters of Measures, *Journal of Mathematical Imaging and Vision*, 51, 22–45.
- Dissmann, J., Brechmann, E. C., Czado, C., and Kurowicka, D. (2013), Selecting and estimating regular vine copulae and application to financial returns, *Computational Statistics & Data Analysis*, 59, 52–69.
- Dziugaite, G. K., Roy, D. M., and Ghahramani, Z. (2015), Training generative neural networks via Maximum Mean Discrepancy optimization, *Proceedings of the Conference on Uncertainty in Artificial Intelligence*, <http://www.auai.org/uai2015/proceedings/papers/230.pdf> (2019-07-26).
- Genest, C., Rémillard, B., and Beaudoin, D. (2009), Goodness-of-fit tests for copulas: A review and a power study, *Insurance: Mathematics and Economics*, 44, 199–213.
- Hofert, M., Kojadinovic, I., Mächler, M., and Yan, J. (2018), Elements of Copula Modeling with R, Springer Use R! Series, ISBN 978-3-319-89635-9, doi:10.1007/978-3-319-89635-9.
- Hofert, M. and Mächler, M. (2014), A graphical goodness-of-fit test for dependence models in higher dimensions, *Journal of Computational and Graphical Statistics*, 23(3), 700–716, doi:10.1080/10618600.2013.812518.
- Hofert, M. and Oldford, R. W. (2018), Visualizing Dependence in High-dimensional Data: An Application to S&P 500 Constituent Data, *Econometrics and Statistics*, 8, 161–183, doi:10.1016/j.ecosta.2017.03.007.
- Hofert, M., Prasad, A., and Zhu, M. (2021a), Multivariate time-series modeling with generative neural networks, *Econometrics and Statistics*, doi:10.1016/j.ecosta.2021.10.011.
- Hofert, M., Prasad, A., and Zhu, M. (2021b), Quasi-random sampling for multivariate distributions via generative neural networks, *Journal of Computational and Graphical Statistics*, 30(3), 647–670, doi:10.1080/10618600.2020.1868302.
- Kingma, D. P. and Ba, J. (2014), Adam: A method for stochastic optimization, <https://arxiv.org/abs/1412.6980> (2022-03-10).
- Li, Y., Swersky, K., and Zemel, R. (2015), Generative moment matching networks, *International Conference on Machine Learning*, 1718–1727.
- Munkres, J. R. (2000), Topology, 2nd ed., Prentice Hall.
- Rosenblatt, M. (1952), Remarks on a Multivariate Transformation, *The Annals of Mathematical Statistics*, 23(3), 470–472.
- Wu, F., Valdez, E. A., and Sherris, M. (2007), Simulating Exchangeable Multivariate Archimedean Copulas and its Applications, *Communications in Statistics – Simulation and Computation*, 36(5), 1019–1034.